crystals

MDPI

Review

Li-rich Layered Oxides: Structure and Doping Strategies to Enable Co-Poor/Co-Free Cathodes for Li-Ion Batteries

Laura Silvestri [1], Arcangelo Celeste [1,2], Mariarosaria Tuccillo [2] and Sergio Brutti [2,*]

[1] Dipartimento di Tecnologie Energetiche e Fonti Rinnovabili, ENEA C.R. Casaccia, Via Anguillarese 301, 00123 Rome, Italy
[2] Dipartimento di Chimica, Sapienza Università di Roma, P.le Aldo Moro 5, 00185 Rome, Italy
* Correspondence: sergio.brutti@uniroma1.it

Abstract: Lithium-rich layered oxides (LRLO) are a wide class of innovative active materials used in positive electrodes in lithium-ion (LIB) and lithium–metal secondary batteries (LMB). LRLOs are over-stoichiometric layered oxides rich in lithium and manganese with a general formula $Li_{1+x}TM_{1-x}O_2$, where TM is a blend of transition metals comprising Mn (main constituent), Ni, Co, Fe and others. Due to their very variable composition and extended defectivity, their structural identity is still debated among researchers, being likely an unresolved hybrid between a monoclinic (mC24) and a hexagonal lattice (hR12). Once casted in composite positive electrode films and assembled in LIBs or LMBs, LRLOs can deliver reversible specific capacities above 220–240 $mAhg^{-1}$, and thus they exceed any other available intercalation cathode material for LIBs, with mean working potential above 3.3–3.4 V vs Li for hundreds of cycles in liquid aprotic commercial electrodes. In this review, we critically outline the recent advancements in the fundamental understanding of the physical–chemical properties of LRLO as well as the most exciting innovations in their battery performance. We focus in particular on the elusive structural identity of these phases, on the complexity of the reaction mechanism in batteries, as well as on practical strategies to minimize or remove cobalt from the lattice while preserving its outstanding performance upon cycling.

Keywords: lithium-rich layered oxides; secondary aprotic batteries; positive electrode materials; Li-ion; cathodes

Citation: Silvestri, L.; Celeste, A.; Tuccillo, M.; Brutti, S. Li-rich Layered Oxides: Structure and Doping Strategies to Enable Co-Poor/Co-Free Cathodes for Li-Ion Batteries. *Crystals* **2023**, *13*, 204. https://doi.org/10.3390/cryst13020204

Academic Editor: Fei Gao

Received: 19 December 2022
Revised: 12 January 2023
Accepted: 18 January 2023
Published: 23 January 2023

1. Introduction

Developing effective and sustainable energy storage is a key societal challenge for the enforcement of reliable collective actions at a world level to mitigate the CO_2 concentration increase in the Earth's atmosphere and possibly to pave the way for its reduction in the second half of this century [1]. Currently, various technologically accessible energy storage devices are on the market, each tackling a specific need and thus filling a specific market niche. As an example, water dams deal with massive energy storage are used to supply power to the energy grids in the consumption peaks, lead–acid batteries are unavoidable power devices used to start internal combustion engines in cars, whereas Li-ion batteries feed energy into all of our innumerable electronic mobile apparatuses [2]. On the other hand, the market diffusion of electric vehicles, as well as the upgrade to the nationwide energy grids to continental-based smart energy networks, is pushing the current energy storage technologies to their limits, thus requiring innovative breakthroughs.

Li-ion batteries (LIBs) are the most remarkable success case in the energy storage technology landscape in the last fifty years: [3] their unique configuration allows for a fine tuning of performance and properties to meet diversified application needs. This is specifically thanks to their flexible combination of positive electrodes/electrolyte/negative electrodes components [4,5]. Since their market presentation in the early 90s, the most limiting performance factors of LIBs deal with costs and the gravimetric-specific capacity

limits. To tackle these drawbacks, the international R&D community has been working hard over the last thirty years to shift from $LiCoO_2$ to high-capacity positive electrode materials, from carbonate-based liquid electrolytes to solid-state ones, and from graphite to high-capacity negative electrode materials [3,6]. Recently, the European Union categorized the various battery chemistries into "generations", starting from the (+)$LiCoO_2$/EC:DMC $LiPF_6$/graphite(−) Generation 1 (i.e., EC = ethylene carbonate, DMC = dimethyl carbonate), and extending to the innovative Generation 3a and 3b (high capacity lithium-ion batteries), Generation 4a (solid-state lithium metal batteries), Generation 4b (lithium–sulphur batteries) and Generation 5 (lithium–oxygen and beyond-lithium batteries) [7]. Currently battery manufacturers are addressing the transition from Generation 2 to Generations 3a and 3b, whereas all next generations are still under development in R&D laboratories worldwide. It is important to underline that the most remarkable bottleneck of generation 3a and 3b is the capacity limitation of positive electrodes, that barely exceed 150 $mAhg^{-1}$ in respect to the mass of the cathode active material. Given this meagre gravimetric performance, it is not surprising that positive electrodes accounts for the majority of the sum of the active material mass (negative + positive sides) in any Li-ion battery (e.g., twice the mass of graphite, five times the mass of tin, twenty times the mass of silicon, with C, Sn and Si being popular negative electrode materials for Li-ion batteries). Thus, any capacity improvement of positive electrode materials highly impacts the overall performance of the entire battery and motivates strong drivers in R&D to develop innovative families of cathode materials (e.g., Ni-rich layered oxides, high-voltage phospho-olivines, fluoro-phosphates) [8–10]. Among these, lithium-rich layered oxides have played a pivotal role in recent years thanks to their compositional flexibility, very high practical capacities exceeding 200–220 $mAhg^{-1}$, satisfactory working potential (3.3–3.6 V vs Li), good environmental compatibility and manufacturing processes similar to those for standard layered oxides [11,12].

Lithium-rich layered oxides (LRLO) are over-stoichiometric oxides rich in lithium and manganese, with the general formula $Li_{1+x}TM_{1-x}O_2$, where TM is a blend of transition metals comprising Mn (main constituent), Ni, Co, Fe and others. Once formulated in positive electrode composite films, these materials demonstrate excellent reversible performance for hundreds of charge/discharge cycles in aprotic lithium–metal and in aprotic lithium-ion batteries: their unique functional properties are rooted in the peculiar composition, structure, and extended disorder at crystalline level. There have been very intense R&D efforts in this field, aiming to develop innovative materials with minor (or even absent) Co-content (cobalt is a critical raw material), capable of delivering high coulombic efficiencies in batteries and high-capacity retentions for thousands of cycles, that can then be manufactured using facile and environmentally feasible protocols.

In this review, we outline the recent advancements in the fundamental understanding of the physico-chemical properties of LRLO as well as the most exciting innovations in their battery performance (see Figure 1). Here, we focus specifically on the analysis of the elusive LRLO crystal structure and de-lithiation/lithiation mechanism in Li-ion batteries, as well as on the strategies to minimize or remove cobalt from the LRLO lattice without damaging the performance.

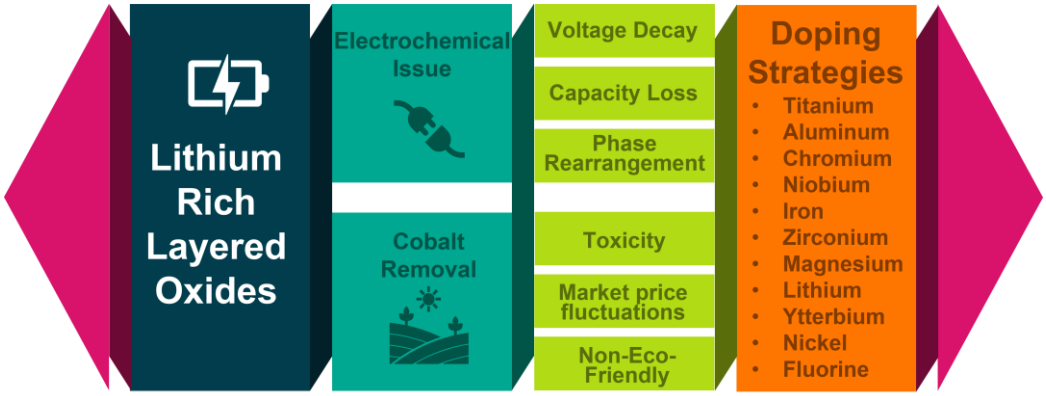

Figure 1. Schematic diagram of topic discussed in this review.

2. Structure and Reaction Mechanism

Li-rich layered oxide (LRLO) cathode materials show an ambiguous crystalline structure, still debated among researchers. The typical X-ray diffraction (XRD) pattern, experimentally observed for any LRLOs, can be indexed with the α-$NaFeO_2$-type structure (see Figure 2a,b) or O3-type. This prototypal structure consists of TMs-based edge-sharing TM-O_6 octahedral (TM = Ni, Co, Mn etc. in 3b site) transition metals layers, separated by layers of Li^+ (3a site), where the oxygen planes (6c site) have an ABCABC stacking sequences and adopt R$\bar{3}$m symmetry (hR12) [13]. However, XRD patterns of all LRLOs reported in the literature also show broad and weak peaks in the 20–30° range (excitation wavelength, Cu Kα) that cannot be indexed by adopting the hR12 lattice. Currently, these diffraction lines are considered clues to the existence of an unresolved superstructure, with Li_2MnO_3 symmetry crystallizing in a monoclinic layered structure, that adopts a C2/m space group (mC24) as reported in Figure 2b [14]. In this lattice, Li ions occupy interslab octahedral sites (4h and 2c) and slab octahedral sites (2b and 4g) together with Mn ions in (1:2) ratio, whereas oxygen atoms occupies 4i and 8j sites. The layered structure of Li_2MnO_3 is often described by using the notation $Li[Li_{1/3}Mn_{2/3}]O_2$, where Mn ions are partially replaced by Li ions and Li^+ and Mn^{4+} form a locally ordered honeycomb structure [15,16].

The above-mentioned superstructure peaks originate from the symmetry-allowed X-ray coherent scattering from lattice-planes, induced by the ordered $LiMn_6$ motifs in the TMs layer. Thus, single-phase Rietveld refinement unavoidably fails to fully achieve an accurate structural reconstruction when assuming either the $R\bar{3}m$ or the $C2/m$ prototype structures (Figure 2c), the real structure being a hybrid intermediate.

Due to these structural peculiarities, there is not a general consensus on the way LRLO lattice is analyzed and discussed in the literature. In most cases, LRLOs have been described by using one between two very popular notations [17]:

(a) $(1\text{-}x)Li_2MnO_3 \cdot xLiMO_2$, as nano-composite of $R\bar{3}m$ and $C2/m$;
(b) $Li_{1+x}M_{1-x}O_2$, as a single solid solution.

According to Thackeray et al. [18], the structure of LRLOs has a composite character consisting of nanometer regions with Li_2MnO_3- and $LiTMO_2$-like features. Bareño et al. [19], through a combination of diffraction, microscopy and spectroscopy, proposed a dendritic microstructure, where $LiCoO_2$- and Li_2MnO_4-like structures coexists. The study on $Li[Li_{0.2}Mn_{0.6}Ni_{0.2}]O_2$, reported by Gu et al. [20], suggested a nanoscale composite with a structural integration of $LiMO_2$ $R\bar{3}m$ phase with Li_2MnO_3 $C2/m$ phase. In particular, by the use of atomic-scale Z-contrast imaging, X-ray energy-dispersive spectroscopy (XEDS) and electron energy loss spectroscopy (EELS), they observed the Ni segregation at the surface layers and grain boundaries, with the concentration increasing gradually from <20% in the inner part of particle to 50% in some superficial regions, while Mn is abundant in the core and deficient in the surface region. Despite oxygen having a more uniform

distribution, an increase in oxygen concentration was observed in the inner part of particles. Furthermore, Aurbach et al. [21,22] investigated a nanoscale composite structure of $0.5Li_2MnO_3$–$0.5LiMn_{1/3}Ni_{1/3}Co_{1/3}O_2$, demonstrating that the rhombohedral $LiNiO_2$-like and monoclinic Li_2MnO_3 structures are integrated and interconnected at the atomic level.

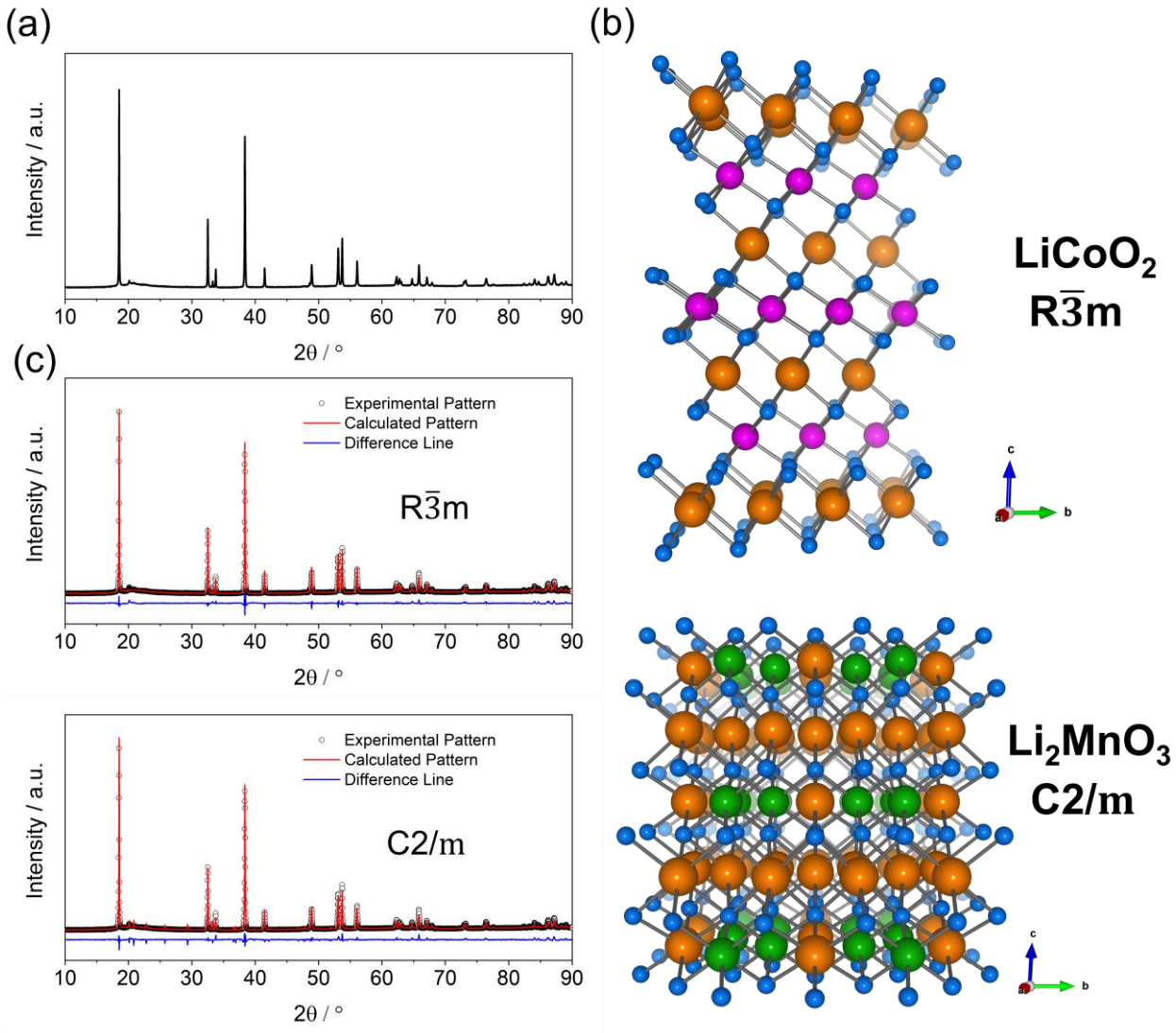

Figure 2. (**a**) XRD pattern of $Li_{1.2}Mn_{0.54}Ni_{0.13}Co_{0.13}O_2$ acquired with a Rigaku SmartLab (Bragg-Brentano geometry, CuKα radiation), (**b**) pictorial structure of $LiCoO_2$ ($R\bar{3}m$ symmetry; ICSD: 74330) and Li_2MnO_3 ($C2/m$ symmetry; ICSD: 165686) where Li and metals layers can be seen. Lithium is orange, Co is pink, Mn is green, and O is blue.(**c**) Rietveld refinement, obtained with GSAS-II of XRD pattern, assuming $R\bar{3}m$ or the $C2/m$ symmetry.

On the contrary, Jarvis et al. [14,20] reported $Li[Li_{0.2}Mn_{0.6}Ni_{0.2}]O_2$ to be a single-phase solid solution with long-range lithium ordering, resulting in a $C2/m$ symmetry since they had no evidence of two-phase behavior. The studies conducted by Lu et al. [23] confirmed that these compounds are true solid solutions of an Li_2MnO_3-like structure. Additionally, Koga et al. [24] affirmed that $Li_{1.2}Mn_{0.54}Co_{0.13}Ni_{0.13}O_2$ has a rhombohedral $R\bar{3}m$ structure with long-range $\sqrt{3}a_{hex} \times \sqrt{3}b_{hex}$ cation ordering using ND and electron diffraction associated with NMR and Raman spectroscopy. The electron diffraction pattern observed along the [1−10] zone axis cannot be considered to be a simple combination or nanocomposite of typical Li_2MnO_3 and $LiMO_2$ materials. These results are in good agreement with the work of Jarvis et al. [25], which reported a monoclinic structure with a significant number

of thin planar defects along (001) planes based on diffraction STEM (D-STEM). Ates et al. [26] confirmed the presence of a single $C2/m$ solid solution using selected-area electron diffraction (SAED), because some of the diffraction patterns can be solely indexed to this phase.

Overall, the large compositional variety of LRLOs and their high defectivity even increases their structural complexity, thus making any facile structure clarification ambiguous and incomplete. In fact, several groups demonstrated the presence of multiple planar defects across the transition metal layers possibly classified as stacking faults [27,28], or interstitials/vancacies/anti-site defects [29,30]. Moreover, structural properties vary with the composition and with the synthetic technique used, from precursor mixing and annealing conditions [31,32].

The structural ambiguity of LRLOs directly reflects on to the sluggish rationalization of the corresponding redox mechanism in batteries and the unsatisfactory comprehension of the structural evolution occurring during repeated cycles of electrochemical lithium-ions extraction/insertion. In Figure 3a, the typical potential profile of the first cycle obtained is shown for an LRLO with the $Li_{1.2}Mn_{0.54}Ni_{0.13}Co_{0.13}O_2$ stoichiometry [33]. The first electrochemical process shows a two-step charge profile: a slope up to 4.4 V, where the Li extraction is balanced by the oxidation of transition metals (Co^{3+}/Co^{4+} and $Ni^{2+}/Ni^{3+}/Ni^{4+}$) and a long plateau above 4.5 V, where the further lithium removal is balanced by the activation of the O^{2-}/O^{-} redox couple [34,35]. The manganese is not involved in this first electrochemical process due to its stability in +4 oxidation state. The potential profile changes drastically after the first charge (Figure 3b), as well as in the following cycles, leading to the so-called voltage (or working potential) decay upon cycling and consequently increasing the voltage hysteresis between charge and discharge. Focusing on the first cycle, it is important to underline that the electrochemical reaction occurring along the 4.5 V vs Li plateau in the first cycle is only partially reversible and disappears during the discharge step. In fact, the reinsertion of Li^+ into the LRLO occurs not only by the exploitation of the Co/Ni/O redox couples but also by the reduction of Mn^{4+} to $Mn^{3+/2+}$ near 2 V [35].

The occurrence of lattice oxygen redox has been proposed in the literature to explain the extra capacity of LRLOs, which extends well beyond that achievable by exploiting the Ni/Co redox couples [36], and the observation of the O_2 release in the first charge high-voltage plateau [37,38]. However, the products of this anionic redox reaction are still objects of discussion. Tarascon's group [39,40] proved the existence of O-O dimers and the formation of reversible O^{2n-} by XPS measurements on $Li_2Ru_{1-y}Mn_yO_3$ and $Li_2Ru_{0.75}Sn_{0.25}O_2$ compounds. Then, Li et al. [41] obtained the direct observation of O^{-}-O^{-} dimers bonding, mostly along the *c*-axis of $Li_{1.2}Ni_{0.2}Mn_{0.6}O_2$. Chen et al. [42] confirmed the formation of oxygen dimerization and the presence of molecular O_2 in Li_2MnO_3 using ab initio techniques. On the other hand, many authors reported the formation of electron holes on oxygen atoms, O^{n-} ($n < 2$), instead of dimer species. In this context, Luo et al. [43,44] demonstrated for the two compounds $Li_{1.2}Mn_{0.54}Ni_{0.13}Co_{0.13}O_2$ and $Li_{1.2}Mn_{0.6}Ni_{0.2}O_2$ that Li^+ removal is charge-compensated by the formation of localized electron holes on O atoms coordinated by Mn^{4+} and Li^+ ions. Conversely, Gent et al. [45] proposed a novel mechanism in which the oxygen redox with the formation of holes is always coupled with transition metals migration, $\{O^{2-} + TM\} \rightarrow \{O^{-} + TM_{mig}\} + e^{-}$.

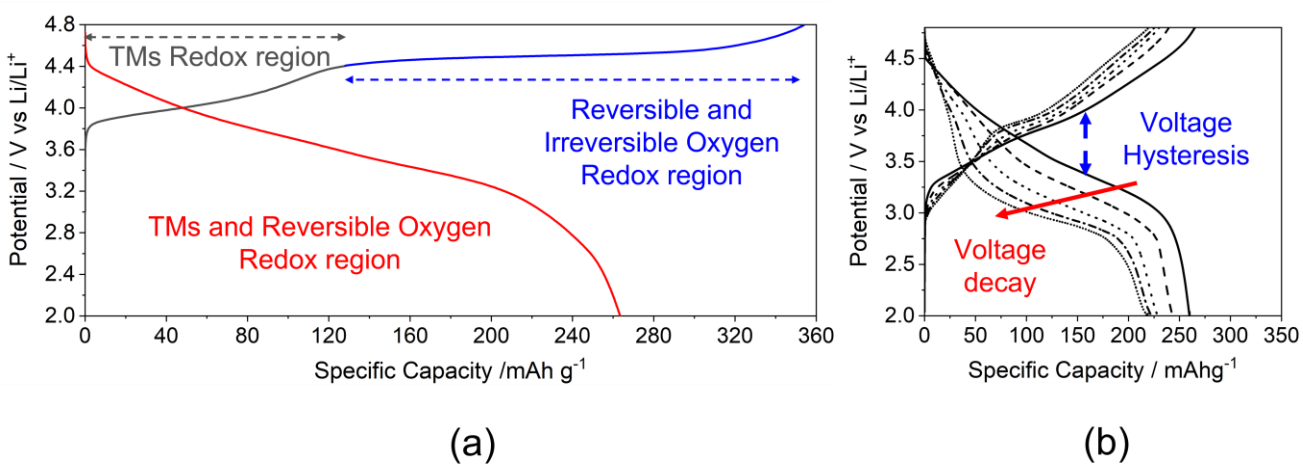

Figure 3. Typical potential profile of LRLOs (**a**) upon first cycle and (**b**) during prolonged cycling.

One direct effect, induced by the molecular oxygen release in the phase composition and the structure of LRLOs after the first charge, is the interdiffusion of metal cations from the bulk to the surface of the single crystal particles, and the consequent phase reorganization (Figure 4) [46,47].

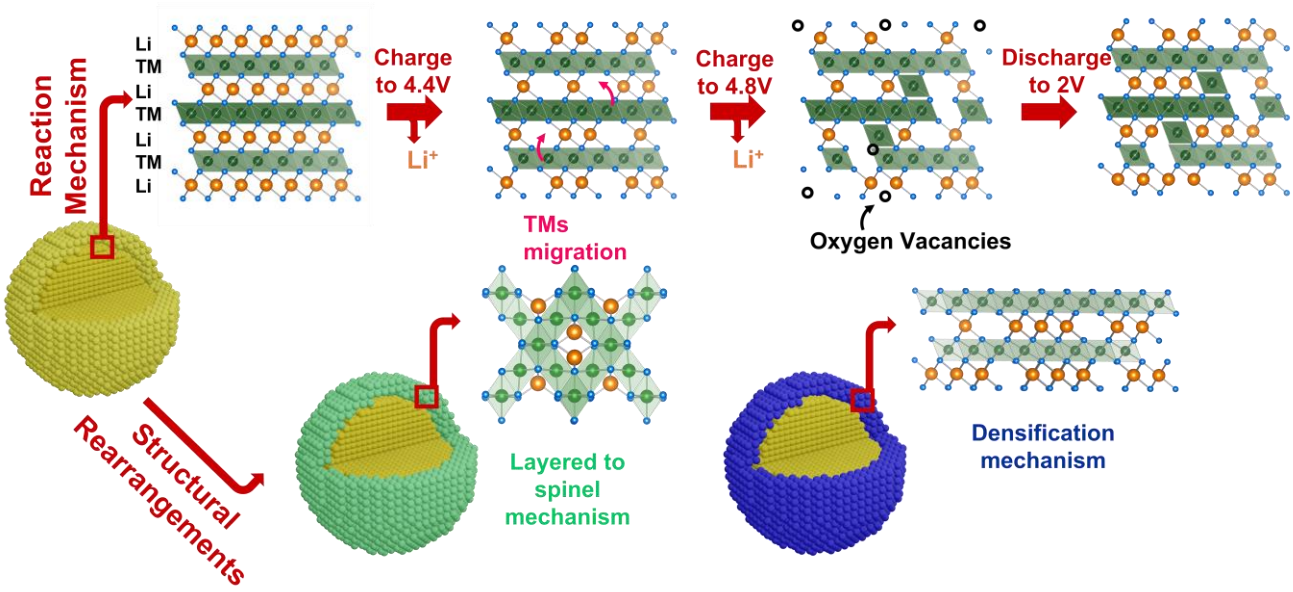

Figure 4. Schematic representation of the reaction mechanism of LRLOs during the electrochemical Li de-intercalation/intercalation and resulting structural changes.

In fact, the oxygen redox activity has different structural effects in the particles bulk and on their surface. When it occurs in the bulk, it is reversible and increases the specific capacity delivered by LRLOs, as demonstrated by Assat et al. with the use of HAXPES technique [48]. Conversely, when the redox activity occurs in proximity to the particle surfaces, this facilitates the irreversible release of molecular oxygen, leaving 0D vacancies in the LRLO anionic sublattice [49]. As a consequence, and unavoidably, the accumulation of oxygen vacancies promotes cation mixing, stacking faults, segregation of new phases and irreversible changes in the oxidation state of metals. This structural degradation mechanism has been analyzed in detail by Cui et al. Supported by XRD, HRTEM and SAED measurement [50], they proposed a multi-step process. The structural degradation

of LRLOs consists of an initial stage associated to the irreversible loss of part of lattice oxygen and the formation of oxygen vacancies on the surface, followed by the migration of transition metal ions into the lithium layer. This interdiffusion results in a further cation mixing and triggers a layered-to-spinel structure transformation. The evidence of the formation of a new spinel-like solid phase on the surface of electrodes after the first charge has also been proved by other groups. Xu et al. [51] investigated the surface changes of the samples before and after electrochemical cycling through electron energy loss spectroscopy (EELS) measurements. Converserly, Boulineau et al. [52] reported the first evidence of Mn-Ni segregation, highlighting the motion of Mn ions from the surface to the bulk, while spinel distortion occurs on the surface with a thickness of about 2–3 nm. Other groups described the phase evolution of LRLOs upon cycling with the occurrence of a material densification and phase degradation, as reported by Armstrong et al. in 2006 [38]. According to this work, as a consequence of the oxygen release, there is the formation of oxygen vacancies near the surface, thus promoting the migration of TM ions from the surface to the bulk to occupy the empty Li octahedral sites in TM layers. The net effect is the densification of manganese and nickel in the octahedral sites in TM layers. Delmas and co-workers [53,54] extensively studied the structural evolution of LRLOs. They confirmed the densification model with ex situ X-ray diffraction during the first cycle. The densified phase grows from the surface while the inner of the particles does not change. Recently, Celeste et al. [55,56] extended the analysis beyond the first cycle on $Li_{1.2}Mn_{0.54}Ni_{0.13}Co_{0.13}O_2$ and $Li_{1.28}Mn_{0.54}Ni_{0.13}Co_{0.02}Al_{0.03}O_2$ using XRD and Raman spectroscopy. From the XRD analysis, the patterns showed the formation of a new phase during the first charge, with a very similar structure to the pristine one. Apparently, both pristine and densified phases can further reversibly exchange lithium ions cycle-by-cycle, while their relative amount changes. Remarkably, Celeste et al. proved using Raman spectroscopy that the appearance of a peak shoulder could possibly be attributed to the spinel distortion. This suggested that even more complex multiphase dynamics are in play, with mechanisms operating from the inner core to outer layers of the primary particles of LRLOs.

3. Open Challenges for the Development of LRLOs

The full comprehension of the structural complexity of LRLOs and of their detailed reaction mechanism is essential to making these materials suitable for the commercialization. As discussed in the previous section, the current consensus is that the extra capacity, delivered by LRLOs beyond the tetravalent oxidation state of transition metal ions, is due to the anion redox reaction. However, the exact nature and identity of the products of this oxygen redox reaction (e.g., superoxidic or peroxidic pairs, de-localized distributed negative charge loss in the anionic sublattice, localized charged vacancies in the lattice, either cationic or anionic) is difficult to reveal and quantify, and is likely interplayed with the long-term cycling behavior of any LRLOs [36]. It is likely that the redox mechanisms involving the oxygen redox couples are related to the local and mean composition of the LRLO. Indeed, it is the nature of the oxidized species to depend closely on the covalency of metal–oxygen bonds [44], the presence of cationic vacancies near the oxygen, the activation of migrations, the existence of charged vacancies in the negative sublattice, the lithium concentration in the TM layer, etc. Furthermore, and unavoidably, any additional O_2 release in the first charge plateau [37,57] is necessarily interplayed with the formation of oxygen vacancies in the structure, the cation mixing, the formation of stacking faults, the segregation of densified new phases and/or the irreversible changes in the oxidation state of metals [58,59]. Remarkably, it is not still clear if these vacancies, or other 0D defects, are either a bulk or a surface phenomenon and if they can migrate from the surface to the bulk or vice-versa. Overall, the redox crystal chemistry and phase phenomena occurring in the electrochemical de-lithiation/lithiation of any LRLO is a very intricate process and, surely, affects the cycling performances and origins of the potential fading upon cycling.

From a structural point of view, the main consequences of the exploitation of the anionic redox activity are a gradual coordination transformation around the TMs layer stacking. The exact degradation mechanisms are not fully understood, and many hypotheses have been discussed and validated on specific LRLO compositions, ranging from a structural shift to form a spinel structure [60,61] to the formation of densified layers [62]. Furthermore, the oxygen loss from the lattice is also interplayed with side reactions with non-aqueous electrolytes during the first de-lithiation, leading to the formation of lithium oxide, lithium carbonate, organic species, and the release of protons in the electrolytes [63]. These undesired electrochemical processes likely contribute to the large irreversible capacity loss and the low Coulombic efficiency observed in the first cycle.

Overall, the development of effective and reliable LRLOs is challenged by a variety of drawbacks which it is important to rationalize and understand in order to improve the initial Coulombic efficiency, mitigate the working potential decay upon cycling and increase the rate performance. Nonetheless, the foreseen competitivity of these materials in the battery market is challenged by the need for optimized manufacturing procedures to reduce the costs of using sustainable supplies of raw materials, and to integrate their production into already existing industrial protocols and infrastructures. In this respect, the removal of cobalt from the structure of LRLOs is a key issue to improving their environmental compatibility, minimizing the need for critical raw materials in the manufacture and reducing the costs [64,65]. Cobalt substitution can be achieved by a balanced blend of other metals. However, any alteration of the metal blend in the transition metal layer has inevitable effects on the electronic and crystallographic structure of the LRLOs as well as on its thermodynamic stability, thus affecting the resulting battery performance. Computational studies suggest that the reduction in the Co content in the LRLO lattice leads to an expansion of the structures due to the greater electronic distortions, i.e., Jahn–Teller defects [66,67]. This structural effect can promote the mobility of lithium ions thanks to weaker coordination but it also promotes the cation interdiffusion and reduces the electronic density of states at the Fermi level, possibly negatively impacting the electronic conductivity [67].

4. Progresses on Doping Strategies for LRLOs

Doping is one of the most used strategies to improve the structural stability, mitigate the voltage fading and reduce the capacity loss of LRLOs. This strategy has also been adopted to reduce, or completely remove, cobalt from the structure. In this paragraph, we summarize current advancements to outline a comprehensive overview about the use of doping to obtain Co-poor or Co-free LRLOs. Table 1 reports the doping strategies and the electrochemical performance discussed in the following paragraphs.

Table 1. Effect of Doping strategies on cathode performance.

Doping Strategies	Stoichiometry	Specific Capacity (mAh g^{-1}) 1st Discharge Cycle	Capacity Retention (%) at Cycle (X)	
Benchmark	$Li_{1.2}Mn_{0.54}Ni_{0.13}Co_{0.13}O_2$	363	76% (200)	[56]
Co-poor				
Ni:Co:Mn Ratio	$Li_{1.15}Ni_{0.32}Co_{0.1}Mn_{0.55}O_2$	282.2	90 % (10)	[68]
	$Li_{1.2}Ni_{0.32}Co_{0.04}Mn_{0.44}O_2$	225	85% (100)	[69]
	$Li[Li_{0.2}Mn_{0.6}Ni_{0.1}Co_{0.1}]O_2$	350	71.4% (100)	[70]
	$Li_{1.2}Mn_{0.51}Ni_{0.0725}Co_{0.0725}O_2$	185.1	98%	[71]

			(100)	
Yb^{3+}	$Li_{1.2}Ni_{0.13}Co_{0.127}Yb_{0.003}\ Mn_{0.54}O_2$	219.8	84.4% (100)	[72]
Ti^{4+}	$Li_{1.167}Ni_{0.36}Mn_{0.383}Co_{0.05}Ti_{0.04}\ O_2$	186.6	99.4% (10)	[73]
Al^{3+}	$Li_{1.14}(Ni_{0.136}Co_{0.10}Al_{0.03}Mn_{0.544})\ O_2$	212	95.65% (100)	[74]
	$Li_{1.2}Ni_{0.15}Mn_{0.55}Co_{0.05}Al_{0.05}O_2$	231.7	98% (30)	[75]
Nb^{5+}	$Li_{1.2}(Ni_{0.13}Co_{0.13}Mn_{0.54})_{0.8}Nb_{0.02}O_2$	287.5	98% (300)	[76]
	$Li_{1.14}Mn_{0.466}Ni_{0.249}Co_{0.046}Al_{0.015}Nb_{0.02}O_2$	207	98% (200)	[77]
Fe^{3+}	$Li_{1.2}Mn_{0.56}Ni_{0.16}Co_{0.04}Fe_{0.04}O_2$	330	82% (80)	[78]
	$Li_{1.2}Mn_{0.56}Ni_{0.16}Co_{0.03}Fe_{0.05}O_2$	108.9	96.1% (100)	[79]
	$Li_{1.2}Ni_{0.133}Mn_{0.534}Co_{0.118}Fe_{0.016}O_2$	87.2	79% (100)	[80]
Cr^{3+}	$Li_{1.2}Ni_{0.16}Mn_{0.56}Co_{0.06}Cr_{0.02}\ O_2$	200	75% (50	[81]
Al^{3+}/Zr^{4+}	$Li[Li_{0.2}Ni_{0.13}Co_{0.13}Mn_{0.54}]_{0.965}Al_{0.02}Zr_{0.015}O_2$	245.5	98% (550)	[82]
Li^{+}/Al^{3+}	$Li_{1.28}Mn_{0.54}Ni_{0.13}Co_{0.02}Al_{0.03}O_2$	264	82% (200)	[83]
Ti^{4+}/Zr^{4+}	$Li_{1.2}Mn_{0.53}Ni_{0.13}Co_{0.13}Ti_{0.01}Zr_{0.01}O_2$	204.1	84% (400)	[84]
PO_4^{3-}	$Li(Li_{0.17}Ni_{0.20}Co_{0.05}Mn_{0.58})O_{1.95}\ (PO_4^{3-})_{0.05}$	252.4		[85]
SiO_4^{4-}/SO_4^{2-}	$Li(Li_{0.17}Ni_{0.20}Co_{0.05}Mn_{0.58})O_{1.95}(SiO_4)_{0.05}$	282.2	71% (400)	[86]
	Co-free			
Li:Ni:Mn ratio	$Li_{1.2}Mn_{0.6}Ni_{0.2}O_2$	155		[87]
	$Li_{1.1}Ni_{0.35}Mn_{0.55}O_2$	160	80% (150)	[88]
Fe^{3+}	$Li_{1.2}Ni_{0.13}Fe_{0.13}Mn_{0.54}O_2$	200	80% (100)	[89]
	$Li_{1.2}Mn_{0.585}Ni_{0.185}Fe_{0.03}O_2$	232	70% (200)	[90]
	$Li(Li_{0.17}Ni_{0.17}Fe_{0.17}Mn_{0.49})O_2$	231.8	73% (100)	[91]
	$Li_{1.16}Ni_{0.19}Fe_{0.18}Mn_{0.46}O_2$	259	83% (100)	[92]
Cr^{3+}	$Li_{1.2}Ni_{0.175}Mn_{0.575}Cr_{0.05}O_2$	225		[93]
Mg^{2+}	$Li[Li_{0.15}Ni_{0.235}Mg_{0.04}Mn_{0.575}]O_2$	127	68% (50)	[94]
	$Li[Li_{0.2}Ni_{0.195}Mn_{0.595}Mg_{0.01}]O_2$	140.6	62% (60)	[95]
Li^{+}/Mn^{4+}	$Li_{1.25}Ni_{0.125}Mn_{0.625}O_2$	185	74% (150)	[96]
F^{-}	$Li_{1.2}Mn_{0.6}Ni_{0.2}O_{1.99}F_{0.01}$	240	95%	[97]

			(100)	
Na^+/PO_4^{3-}	$Li_{1.2}Mn_{0.6}Ni_{0.2}O_2Na_{0.01}(PO_4)_{0.01}$	264.7	86.7% (150)	[98]
Fe^{3+}/Cl^-	$Li_{1.2}Mn_{0.585}Ni_{0.185}Fe_{0.03}O_{1.98}Cl_{0.02}$	183.9	86.4% (500)	[99]

4.1. Co-Poor LRLOs

Cobalt substitution is a remarkable challenge that unbalances the electronic structure and alters the thermodynamic stability of LRLOs. As an example, Kou et al. [68] showed the negative effects of the reduction of cobalt content on the discharge capacities and working voltages of a homologous series of LRLOs with general formula $Li_{1.2}Ni_{0.2-x}Co_{2x}Mn_{0.6-x}O_2$ (x = 0–0.05). In recent years, many different doping strategies or compositions have been investigated to prove the feasibility of Co-free or Co-poor LRLOs with promising performances from il LIBs.

One of the most studied stoichiometry of LRLOs is $Li_{1.2}Mn_{0.54}Ni_{0.13}Co_{0.13}O_2$ and it is often used as a benchmark point for understanding the impact of the reduction of cobalt by changing the Ni:Co:Mn ratio or by introducing new elements. Ramesha et al. [69] prepared a series of LRLOs materials by varying the Ni, Mn and Co contents to identify the optimal ratio. In particular, $Li_{1.2}Ni_{0.32}Co_{0.04}Mn_{0.44}O_2$ shows very small voltage decay and a capacity retention of 85% after 100 cycles. Redel et al. [70] investigated various stoichiometries, $Li[Li_yMn_{1-y-2z}Ni_zCo_z]O_2$, aiming at the reduction of cobalt: the stoichiometry $Li[Li_{0.2}Mn_{0.6}Ni_{0.1}Co_{0.1}]O_2$ showed the best compromise between Co amount and electrochemical properties. In fact, the specific capacities and lithium diffusion coefficients decrease too much when cobalt is less than 0.1 in the structure. Hamad et al. [71] studied the interplay of cobalt and nickel contents in the LRLO by systematically studying a homologue series of materials with stoichiometry $Li_{1.2}Mn_{0.51}Ni_{0.145+x}Co_{0.145-x}O_2$ (x = 0, 0.0725). Despite the initial drop in the specific capacity, the Co-poor sample had an activated trend in the first charge/discharge cycles, with better capacity retention at the end of the test compared to the Co-rich. The superior performance in $Li_{1.2}Mn_{0.51}Ni_{0.0725}Co_{0.0725}O_2$ was attributed to the continuous activation of the Li_2MnO_3 lattice.

Besides altering the Co:Mn:Ni relative ratios, cobalt reduction can be achieved by isovalent or aliovalent doping with other cations. As an example, Bao et al. [72] proposed a series of Yb-doped lithium-rich materials, $Li_{1.2}Ni_{0.13}Co_{0.13-x}Yb_xMn_{0.54}O_2$. The best materials obtained, with x = 0.005, exhibited a discharge capacity of 250.3 and 219.8 $mAhg^{-1}$ at 0.2 and 1C, respectively. Capacity retentions were 87.3 and 84.4% after 50 cycles at 0.2 C and 100 cycles at 1C. Kou et al. [73] prepared a series of Ti-doped, Co-poor, lithium-rich $Li_{1.167}Ni_{0.4-x}Mn_{0.383}Co_{0.05}Ti_xO_2$ (x = 0, 0.02, 0.04 and 0.08). Ti doping has an impact on electrochemical performance and the doped material with x = 0.04 showed the best performance. It had a discharge capacity of 187 $mAhg^{-1}$, with a capacity retention of 99.4% after 10 cycles at 0.1 C.

Among other methods, aluminium doping has been extensively used by many authors. Guo et al. [74] proposed an Al-doped material with formula $Li_{1.14}(Ni_{0.136}Co_{0.10}Al_{0.03}Mn_{0.544})O_2$ in close comparison to the Co-rich $Li_{1.14}(Ni_{0.136}Co_{0.136}Mn_{0.544})O_2$. The doped samples showed a slight decrease in discharge capacity but also improved cycling stability due to the apparent stabilization of the overall structure. Thang et al. [75] used the sol–gel process to synthetize $Li[Li_{0.2}Ni_{0.15}Mn_{0.55}Co_{0.1-x}Al_x]O_2$ (x = 0, 0.025, 0.05, 0.075), reporting the optimum content of Al to be about 0.05. In fact, the $Li_{1.2}Ni_{0.15}Mn_{0.55}Co_{0.05}Al_{0.05}O_2$ stoichiometry can achieve 237 $mAhg^{-1}$ and showed an improved structural stability. Additionally, niobium has been evaluated as a doping element and proven to be able to mitigate the discharge voltage decay, decrease the charge-transfer resistance, and improve the lithium-ion diffusion coefficient. Dong et al. [76] used solvothermal method to prepare a homologue series of LRLOs with general stoichiometry $Li_{1.2}(Ni_{0.13}Co_{0.13}Mn_{0.54})_{1-x}Nb_xO_2$, where x = 0, 0.01, 0.02,

0.04. Samples with Nb amounts equal to 0.02 can achieve a specific capacity of 271 $mAhg^{-1}$ and a capacity retention of 98% after 300 cycles. Dong et al. also proved that Nb can effectively stabilize the crystal structure and improve the charge transfer resistance upon cycling. Recently, Liu et al. [77] confirmed the beneficial effects of Nb traces in Co-poor LRLOs by demonstrating an optimized LRLO stoichiometry, namely $Li_{1.14}Mn_{0.466}Ni_{0.249}Co_{0.046}Al_{0.015}Nb_{0.02}O_2$. This material apparently exhibited excellent electrochemical performance as Nb doping improved the first cycle reversibility, leading to a remarkable capacity retention of 93% after 200 cycles.

Iron is an earth-abundant element and is one of the best choices to replace cobalt thanks to its limited cost and +3 stable oxidation state, like aluminium ions: in fact, many authors have demonstrated its ability to stabilize the electrochemical behaviour of LRLOs. Nayak et al. [78] used iron to partly replace cobalt, obtaining a material with formula $Li_{1.2}Mn_{0.56}Ni_{0.16}Co_{0.04}Fe_{0.04}O_2$. The doped material can deliver a specific capacity of 254 $mAhg^{-1}$ and showed better rate capability and better structural stability than the Co-rich benchmark. More recently, Yi et al. [79] synthetized a series of materials with general stoichiometry $Li_{1.2}Mn_{0.56}Ni_{0.16}Co_{0.08-x}Fe_xO_2$ (x = 0, 0.01, 0.03, 0.05, 0.08), and observed that the reversible capacity of the doped samples is larger compared to the undoped benchmark at very high current density. In particular, the sample x = 0.05, $Li_{1.2}Mn_{0.56}Ni_{0.16}Co_{0.03}Fe_{0.05}O_2$, showed the best performance with minor charge transfer resistance and enhanced Li-ion diffusion. Medvedeva et al. [80] prepared an iron-doped material, i.e., $Li_{1.2}Ni_{0.133}Mn_{0.534}Co_{0.118}Fe_{0.016}O_2$ with excellent capacity retention, thus confirming the strong mitigation of the voltage decay induced by the incorporation of the isovalent iron as a dopant. After 100 charge/discharge cycles, the discharge voltage potentials are 3.3V and 3 V, for doped and undoped samples, respectively, indicating the beneficial effect of iron in improving the structural resilience of LRLO upon cycling.

On the other hand, Nisar et al. [81] successfully synthetized various Cr-doped lithium-rich phases, i.e., $Li_{1.2}Ni_{0.16}Mn_{0.56}Co_{0.08-x}Cr_xO_2$ (where x = 0.00, 0.01, and 0.02), using the sol–gel method. Apparently, chromium doping stabilizes the electrochemical performance in prolonged galvanostatic tests as well as the interface stability between material and electrolyte.

Co-doping has also been used in recent years to exploit synergistic effects arising from the simultaneous presence of two dopants. Ghorbanzadeh et al. [82] proposed Al/Zr co-doping in LRLO, i.e., $Li[Li_{0.2}Ni_{0.13-x+y/3}Co_{0.13-x+y/3}Mn_{0.54-x+y/3}]Al_xZr_yO_2$ (x = 0, 0.02, 0.03 and y = 0, 0.015, 0.03). They demonstrated that the presence of Al improves the structural stability, while the Zr enhances the specific capacity and the lithium diffusion. Celeste et al. [55] focused on the substitution of cobalt with lithium (over-lithiation) and aluminium, leading to a family of materials with general formula $Li_{1.2+x}Mn_{0.54}Ni_{0.13}Co_{0.13-x-y}Al_yO_2$, where $0.03 \leq x \leq 0.08$ and $0.03 \leq y \leq 0.05$. Apparently, the decrease in the cobalt content leads to an expansion of the unit cell due to the enormous difference in the ionic radius of Co^{3+} and Li^+. Concerning the electrochemical behaviour, the potential profiles highlight an alteration of the two-stage redox reaction in the first charge (slope below 4.4 V followed by the long pseudo-plateau at 4.5 V ve Li). Overall, the capacity delivered from the oxidation of transition metals decreases due to the redox inactivity of lithium and aluminium, while the increase in the ionicity of the metal–oxygen bonds partially decrease the extent of the high-voltage plateau. The combination of these two effects leads to a net increase in the first cycle coulombic efficiency. Furthermore, despite the reduction in the overall delivered capacity, all samples can reversibly exchange specific capacities over 200 $mAhg^{-1}$, showing outstanding cycling stability.

The impact of pseudo n-doping on the LRLO crystal and electronic structures has been elucidated by comparing the performance and properties of $Li_{1.28}Mn_{0.54}Ni_{0.13}Co_{0.02}Al_{0.03}O_2$ in close comparison with a Co-rich material, namely $Li_{1.2}Mn_{0.54}Ni_{0.13}Co_{0.13}O_2$ [83]. The replacement of Co with Al and Li leads to the occurrence of native oxygen vacations and changes in the electronic structure. In fact, XANES measurements demonstrated an increase in the net oxidation state of the nickel centres with

the formation of a small amount of Ni^{3+}, additionally showing an increase in the Jahn−Teller defects compared to the Co-rich sample. The most relevant beneficial effect of this strategy is the remarkable reduction in the voltage decay: this behaviour can be correlated to the improvement in the LRLO structure stability upon cycling. In fact, post-mortem XRD patterns and Raman spectra showed the superior structural retention of $Li_{1.28}Mn_{0.54}Ni_{0.13}Co_{0.02}Al_{0.03}O_2$ compared to $Li_{1.2}Mn_{0.54}Ni_{0.13}Co_{0.13}O_2$. Feng et al. [84] used Ti and Zr co-doping to hinder oxygen losses during the first charge: the optimized material has an initial Coulombic efficiency of 84.2% and a suppressed voltage decay. Furthermore, the specific capacity is 229 $mAhg^{-1}$ with a capacity retention of 84% over 400 cycles.

Also anionic doping has been considered and demonstrated to stabilize Co-poor LRLOs. Zhang et al. [85] used PO_4^{3-} polyanions doping in $Li(Li_{0.17}Ni_{0.20}Co_{0.05}Mn_{0.58})O_2$ to partly replace oxygen. In particular, $Li(Li_{0.17}Ni_{0.20}Co_{0.05}Mn_{0.58})O_{1.95}$ $(PO_4^{3-})_{0.05}$ showed improvements in stability and in the discharge midpoint potential. Also SiO_4^{4-} and SO_4^{2-} polyanions with a large radius have been introduced into LRLOs by Zhang et al. [86] showing larger Coulombic efficiencies in the first cycle and enhanced energy retention upon cycling, as confirmed by the minor voltage decay in 400 cycles. In fact, after 400 cycles, the discharge capacities of $Li(Li_{0.17}Ni_{0.20}Co_{0.05}Mn_{0.58})O_{1.95}(SiO_4)_{0.05}$ and $Li(Li_{0.17}Ni_{0.20}Co_{0.05}Mn_{0.58})O_{1.97}(SO_4)_{0.03}$ sample are at 200.4 and 215.4 $mAhg^{-1}$, respectively, approximately 30% larger compared to $Li(Li_{0.17}Ni_{0.20}Co_{0.05}Mn_{0.58})O_2$ (159.9 $mAhg^{-1}$).

4.2 Co-Free LRLOs

Among all the possible Co-free LRLO stoichiometries, $Li_{1.2}Mn_{0.6}Ni_{0.2}O_2$ [100] is the most studied one. Amine et al. [87] proved that this material can exchange 240 $mAhg^{-1}$ with anodic potential cutoff as high as 4.6V vs Li, but with limited reversibility since specific capacity of the first discharge is only of 155 $mAhg^{-1}$. However, the reversible specific capacity showed an activated trend being the discharge capacity at cycle 10 as large as 205 $mAhg^{-1}$. More recently, Manthiram et al. [101] demonstrated how the synthesis conditions and calcination temperatures/duration can enhance the electrochemical performance of $Li_{1.2}Mn_{0.6}Ni_{0.2}O_2$.

Turning to other Co-free stoichiometries, Prakasha et al. [88] investigated the effect of the calcination temperature on the structural properties and the electrochemical performance of an LRLO with composition $Li_{1.1}Ni_{0.35}Mn_{0.55}O_2$. This material was synthesized by the use of spray-pyrolysis combined with a calcination at 900 °C. Once casted in composite electrodes, this active material was able to deliver capacities of 180 and 100 $mAhg^{-1}$ at current rates of C/10 and 1C. A rationalization of the impact of the annealing temperature on transport properties was proposed by Tuccillo et al. using DFT and partially-disordered supercells: apparently the formation of large concentration of Ni/Li antisite defects between TM and Li layers can easily occur at temperatures larger than 700 °C [29].

Additionally, in the case of Co-free LRLOs, isovalent and aliovalent metal doping (including Na^+, Nd^{3+}, Al^{3+}, Fe^{3+}, F^-, S^{2-}, SO_4^{2-} and PO_4^{3-}) was used as effective strategy to improve structural stability and decrease voltage decay upon long-term cycling. For instance, Manthiram et al. [102,103] reported a systematic study into the influence of cationic substitution on the reversible capacity of the first cycle. Manthiram suggested the possible inhibition of an oxygen redox reaction by a tailored doping of the LRLO lattice. Specifically, they considered the substitution of Mn in $Li_{1.2}Mn_{0.6-x}Ni_{0.2}M_xO_2$ with Ti and Mg and the substitution of Mn/Ni in equal amount in $Li_{1.2}Mn_{0.6-0.5x}Ni_{0.2-0.5x}M_xO_2$ with Fe, Al, Cr and Ga. Using this strategy, Manthiram demonstrated that the oxygen redox reaction and the extent of the first cycle high-voltage plateau both decrease by increasing the covalency of metal–oxygen bonds in the lattice.

Laisa et al. [89] proved the enhancement of the functional properties in batteries of the parent $Li_{1.2}Mn_{0.54}Ni_{0.13}Co_{0.13}O_2$ materials by the complete substitution of Co^{3+} with Fe^{3+}. Both the Co- and Fe- LRLOs showed capacity exceeding 300 $mAhg^{-1}$ in the first lithium de-insertion, but the reversibility of the Fe- LRLO was apparently doubled. In the same way, Wu et al. [90] used different contents of iron in a series of LRLOs with general

formula $Li_{1.2}Mn_{0.6-x/2}Ni_{0.2-x/2}Fe_xO_2$ (x = 0, 0.01, 0.03, 0.05) to prove that the capacity decrease, occurring while removing cobalt, can be compensated by an optimized iron content. As such, they obtained an excellent first discharge capacity (~232 $mAhg^{-1}$) and reduced potential fading upon cycling thanks to the suppression of Ni-ion migration from the TM layer to the Li one. Wei et al. [91] determined, using computational and experimental techniques, that the presence of Fe^{3+} in the LRLO lattice contributes to stabilize oxidized oxygen species in particular by avoiding the accumulation of dimers, thus enhancing the structural stability of the de-lithiated LRLO. Recently, Pham et al. [92], by combining operando OEMS (on-line mass spectrometry) and EIS (electrochemical impedance spectroscopy) experiments, proved the gas evolution of CO_2, O_2 and POF_3 upon the first charge and matched the gaseous release with interface resistance modification at the cathode-electrolyte interface for an iron-doped LRLO with formula $Li_{1.16}Ni_{0.19}Fe_{0.18}Mn_{0.46}O_2$. Their study showed that the mitigation of oxygen evolution reaction can decrease the layered-to-spinel transition on the surface of the active material primary particles, thus leading to improved electrochemical performance upon cycling in half-cells.

Chromium doping was investigated by Dahn et al. [23,93] that systematically analysed a series of LRLO with general formula $Li[Cr_xLi_{(1/3-x/3)}Mn_{(2/3-2x/3)}]O_2$ (where x= 0, 1/6, 1/4, 1/3, 1/2, 2/3, 5/6, and 1). Apparently, by a fine tuning of the chromium content, it is possible to stabilize a reversible specific capacity of 230 $mAhg^{-1}$ with a mitigated loss of molecular oxygen. On the other hand, Lee et al. [104] focused on the evaluation of the effect of Cr substitution on the voltage decay of the $Li_{1.2}Ni_{0.2-x/2}Mn_{0.6-x/2}Cr_xO_2$ (x = 0, 0.05, 0.1, and 0.2) series. Apparently, the substitution of Ni/Mn with the redox active Cr, on the one hand, increases the amount of Li^+ de-intercalated from the sloping region thanks to the contribution of the redox couple $Cr^{3+/6+}$, but at the same time decreases the LRLO structural stability due to the formation of Cr^{6+} centres and the distortion of the local coordination around the oxidized TM from octahedra to tetrahedra.

Sun et al. [94] investigated the effect of Mg^{2+} in replacing the Ni^{2+} in $Li[Li_{0.15}Ni_{0.275-x}Mg_xMn_{0.575}]O_2$. The Mg-doped LRLO showed an activated potentials profile and after 50 cycles the specific capacities are 187, 185 and 183 $mAhg^{-1}$, respectively, for x= 0, 0.02, and 0.04. Furthermore, the substitution of Ni^{2+} with the smaller size Mg^{2+} ions increased the structural stability without hindering the Li de-intercalation/intercalation from/into the lattice. Additionally, Wang et al. [95] focused on the evaluation of the effect of Mg doping on a $Li_{1.2}Ni_{0.2}Mn_{0.6}O_2$ cathode and confirmed that the addition of moderate amounts of Mg can stabilize the structure, keep high-capacity performance and increase ionic conductivity (e.g., the sample with 1% of Mg substitution of the Ni/Mn showed a discharge capacity of 226.5 $mAhg^{-1}$ after 60 cycles).

The effect of a simultaneous co-doping in a Co-free LRLO has been less thoroughly explored. Celeste et al. [96] investigated the substitution of Ni from $Li_{1.2}Mn_{0.6}Ni_{0.2}O_2$ by the addition of Li- and Mn-, and optimized a material with formula $Li_{1.25}Ni_{0.125}Mn_{0.625}O_2$. The over-lithiation apparently suppressed the first cycle high-voltage plateau without major effects on the reversible capacity: during the first 50 cycles, the optimized material showed an activated capacity trend and stabilized at 230 $mAhg^{-1}$ at C/10 (40 mAg^{-1}).

Moving to anionic doping, Vanaphuti et al. [97] explored the effect of the incorporation of different anions (F^-, S^{2-} and Cl^-) in the lattice of a $Li_{1.2}Mn_{0.6}Ni_{0.2}O_2$ LRLO. They proved that, among all anionic dopants, F^- increases the mean working potential, improves ionic conductivity, reduces cation mixing, and minimizes oxygen release. The LRLO phase, doped with 1% of fluorine anions, showed a 95% retention capacity after 100 cycles. Liu et al. [98] synthetized $Li_{1.2}Mn_{0.6}Ni_{0.2}O_2$ doped with PO_4^{3-} and co-doped Na^+/PO_4^{3-}. Double anion/cation doping promotes cycle stability, with a capacity retention of 86.7% after 150 cycles and a good rate performance with 153 mAh g^{-1} at 5C. The authors claimed that this strategy suppresses the spinel transformation and improves the structural stability upon cycling. Additionally, Nie et al. [99] used cation/anion co-doping of $Li_{1.2}Mn_{0.6}Ni_{0.2}O_2$ with Fe and Cl and optimized the $Li_{1.2}Mn_{0.585}Ni_{0.185}Fe_{0.03}O_{1.98}Cl_{0.02}$ composition. They demonstrated that balanced co-doping promotes lithium diffusion kinetic

and reduces the oxygen redox reactivity, resulting in improved Coulombic efficiency, better rate performance and long-term stability.

5. Conclusions

Li-rich layered oxides are amongst the best alternative positive electrode active materials for the design and production of next-generation Li-ion batteries (i.e., generation 4a), thanks to their possessing large specific capacities (>250 $mAhg^{-1}$) and the highest specific energy (up to 900 $WhKg^{-1}$) among all intercalation cathodes. LRLOs combines these excellent electrochemical properties with an improved environmental benignity, derived from the large content of manganese in their composition and the facile modification of the stoichiometry to reduce or remove cobalt. However, working potential fading, structural re-organization upon cycling, small Coulombic efficiency and unsatisfactory rate performance still hinder their transition from laboratory to manufacture and therefore the commercialization. As highlighted above, many of these drawbacks are rooted in the complexity of their crystal structure and the elusive electrochemical reaction mechanisms involved in cycling in batteries. Large efforts are still spent worldwide to shed light on these fundamental features of LRLO: currently many discrepancies are still debated in literature and various hypothesis have been experimentally validated concerning both the crystal structure and the de-lithiation/lithiation mechanism. Apparently, the variability of the possible LRLO composition, as well as the thermodynamic facility to incorporate defects into their structures, makes the process of generating a unified model for the interpretation of both aspects complex.

The most relevant benefit of LRLO compared to stoichiometric layered phases (either Mn-rich, Ni-rich or balanced) is the possibility of completely removing cobalt from their lattice without there being major impacts on the resulting electrochemical performance. This result can be obtained by a synergistic strategy that involves the optimization of the material preparation and a balanced cobalt substitution with other isovalent/aliovalent redox/non-redox cations. In fact, the use of different metal blends in the TM lattice, the optimization of the annealing temperatures, the incorporation of cationic or anionic dopants as well as the use of coatings can alleviate the de-stabilization of the lattice induced by Co^{3+} removal. Apparently, many different doping strategies have been proposed in the literature, demonstrating various successful strategies to mitigate the fading of working potential and to increase the structural resilience upon cycling LRLO. Additionally, in this case, a generalized rationale is still missing, which is again likely due to the very wide variety of LRLO composition as well as the lack of a clear structural comprehension of these materials.

Author Contributions: L.S., A.C., M.T. and S.B. have all been involved in drafting this review. A.C. discussed deeply Co-poor LRLOs doping. M.T. discussed Co-free LRLOs. L.S. conceptualization. S.B. review and editing. All authors have read and agreed to the published version of the manuscript.

Funding: L.S. received funds from Ministry of Ecological Transition in the framework of "Ricerca di Sistema Elettrico". The research project here reported was supported by the "Centro Nazionale per la Mobilità Sostenibile (MOST) CN4 Spoke 13 Batterie e Trazione Elettrica" funded by the Italian Government and the European Union in the frame of the "Missione 4 Componente 2 Investimento 1.4 -Potenziamento strutture di ricerca e creazione di "campioni nazionali di R&S" su alcune Key Enabling Technologies del PNRR (Avviso MUR n.3138 del 16-12-2021)".

Data Availability Statement: Not applicable

Conflicts of Interest: The authors declare no conflict of interest.

References

1. Haas, J.; Cebulla, F.; Cao, K.; Nowak, W.; Palma-Behnke, R.; Rahmann, C.; Mancarella, P. Challenges and Trends of Energy Storage Expansion Planning for Flexibility Provision in Low-Carbon Power Systems—A Review. *Renew. Sustain. Energy Rev.* **2017**, *80*, 603–619.

2. Winfield, M.; Shokrzadeh, S.; Jones, A. Energy Policy Regime Change and Advanced Energy Storage: A Comparative Analysis. *Energy Policy* **2018**, *115*, 572–583. https://doi.org/10.1016/j.enpol.2018.01.029.
3. Camargos, P.H.; dos Santos, P.H.J.; dos Santos, I.R.; Ribeiro, G.S.; Caetano, R.E. Perspectives on Li-Ion Battery Categories for Electric Vehicle Applications: A Review of State of the Art. *Int. J. Energy Res.* **2022**, *46*, 19258–19268.
4. Zubi, G.; Dufo-López, R.; Carvalho, M.; Pasaoglu, G. The Lithium-Ion Battery: State of the Art and Future Perspectives. *Renew. Sustain. Energy Rev.* **2018**, *89*, 292–308.
5. Grey, C.P.; Hall, D.S. Prospects for Lithium-Ion Batteries and beyond—A 2030 Vision. *Nat. Commun.* **2020**, *11*, 6279.
6. Finegan, D.P.; Squires, I.; Dahari, A.; Kench, S.; Jungjohann, K.L.; Cooper, S.J. Machine-Learning-Driven Advanced Characterization of Battery Electrodes. *ACS Energy Lett.* **2022**, *7*, 4368–4378. https://doi.org/10.1021/acsenergylett.2c01996.
7. Bielewski, M.; Pfrang, A.; Bobba, S.; Kronberga, A.; Georgakaki, A.; Letout, S.; Grabowska, M. *Clean Energy Technology Observatory, Batteries for Energy Storage in the European Union : Status Report on Technology Development, Trends, Value Chains and Markets*; Publications Office of the European Union: Luxembourg, Luxembourg, 2022.
8. Tolganbek, N.; Yerkinbekova, Y.; Kalybekkyzy, S.; Bakenov, Z.; Mentbayeva, A. Current State of High Voltage Olivine Structured $LiMPO_4$ Cathode Materials for Energy Storage Applications: A Review. *J. Alloys Compd.* **2021**, *882*, 160774.
9. Casas-Cabanas, M.; Ponrouch, A.; Palacín, M.R. Blended Positive Electrodes for Li-Ion Batteries: From Empiricism to Rational Design. *Isr. J. Chem.* **2021**, *61*, 26–37.
10. Mohamed, N.; Allam, N.K. Recent Advances in the Design of Cathode Materials for Li-Ion Batteries. *RSC Adv.* **2020**, *10*, 21662–21685.
11. Nie, L.; Chen, S.; Liu, W. Challenges and Strategies of Lithium-Rich Layered Oxides for Li-Ion Batteries. *Nano Res.* **2022**, *16*, 391–402.
12. Yang, J.; Niu, Y.; Wang, X.; Xu, M. A Review on the Electrochemical Reaction of Li-Rich Layered Oxide Materials. *Inorg. Chem. Front.* **2021**, *8*, 4300–4312. https://doi.org/10.1039/D1QI00687H.
13. Li, W.; Song, B.; Manthiram, A. High-Voltage Positive Electrode Materials for Lithium-Ion Batteries. *Chem. Soc. Rev.* **2017**, *46*, 3006–3059.
14. Jarvis, K.A.; Deng, Z.; Allard, L.F.; Manthiram, A.; Ferreira, P.J. Understanding Structural Defects in Lithium-Rich Layered Oxide Cathodes. *J. Mater. Chem.* **2012**, *22*, 11550–11555. https://doi.org/10.1039/c2jm30575e.
15. Hwang, J.; Myeong, S.; Jin, W.; Jang, H.; Nam, G.; Yoon, M.; Kim, S.H.; Joo, S.H.; Kwak, S.K.; Kim, M.G.; et al. Excess-Li Localization Triggers Chemical Irreversibility in Li- and Mn-Rich Layered Oxides. *Adv. Mater.* **2020**, *32*, e2001944. https://doi.org/10.1002/adma.202001944.
16. Boulineau, A.; Croguennec, L.; Delmas, C.; Weill, F. Reinvestigation of Li_2MnO_3 Structure: Electron Diffraction and High Resolution TEM. *Chem. Mater.* **2009**, *21*, 4216–4222. https://doi.org/10.1021/cm900998n.
17. Hong, J.; Gwon, H.; Jung, S.-K.; Ku, K.; Kang, K. Review—Lithium-Excess Layered Cathodes for Lithium Rechargeable Batteries. *J. Electrochem. Soc.* **2015**, *162*, A2447–A2467. https://doi.org/10.1149/2.0071514jes.
18. Thackeray, M.M.; Johnson, C.S.; Vaughey, J.T.; Li, N.; Hackney, S.A. Advances in Manganese-Oxide "composite" Electrodes for Lithium-Ion Batteries. *J. Mater. Chem.* **2005**, *15*, 2257–2267. https://doi.org/10.1039/b417616m.
19. Wen, J.G.; Bareño, J.; Lei, C.H.; Kang, S.H.; Balasubramanian, M.; Petrov, I.; Abraham, D.P. Analytical Electron Microscopy of $Li_{1.2}Co_{0.4}Mn_{0.4}O_2$ for Lithium-Ion Batteries. *Solid State Ion.* **2011**, *182*, 98–107. https://doi.org/10.1016/j.ssi.2010.11.030.
20. Gu, M.; Genc, A.; Belharouak, I.; Wang, D.; Amine, K.; Thevuthasan, S.; Baer, D.R.; Zhang, J.G.; Browning, N.D.; Liu, J.; et al. Nanoscale Phase Separation, Cation Ordering, and Surface Chemistry in Pristine $Li_{1.2}Ni_{0.2}Mn_{0.6}O_2$ for Li-Ion Batteries. *Chem. Mater.* **2013**, *25*, 2319–2326. https://doi.org/10.1021/cm4009392.
21. Amalraj, F.; Kovacheva, D.; Talianker, M.; Zeiri, L.; Grinblat, J.; Leifer, N.; Goobes, G.; Markovsky, B.; Aurbach, D. Integrated Materials $XLi_2MnO_3 \cdot (1-x)LiMn_{1/3}Ni_{1/3}Co_{1/3}O_2$ (X = 0.3, 0.5, 0.7) Synthesized. *J. Electrochem. Soc.* **2010**, *157*, A1121. https://doi.org/10.1149/1.3463782.
22. Nayak, P.K.; Yang, L.; Pollok, K.; Langenhorst, F.; Aurbach, D.; Adelhelm, P. Investigation of $Li_{1.17}Ni_{0.20}Mn_{0.53}Co_{0.10}O_2$ as an Interesting Li- and Mn-Rich Layered Oxide Cathode Material through Electrochemistry, Microscopy, and In Situ Electrochemical Dilatometry. *ChemElectroChem* **2019**, *6*, 2812–2819. https://doi.org/10.1002/celc.201900453.
23. Lu, Z.; Chen, Z.; Dahn, J.R. Lack of Cation Clustering in $Li[Ni_xLi_{1/3-2x/3}Mn_{2/3-x/3}]O_2$ ($0 < x \leq 1/2$) and $Li[Cr_xLi_{(1-x)/3}Mn_{(2-2x)/3}]O_2$ ($0 < x < 1$). *Chem. Mater.* **2003**, *15*, 3214–3220. https://doi.org/10.1021/cm030194s.
24. Koga, H.; Croguennec, L.; Mannessiez, P.; Ménétrier, M.; Weill, F.; Bourgeois, L.; Duttine, M.; Suard, E.; Delmas, C. $Li_{1.20}Mn_{0.54}Co_{0.13}Ni_{0.13}O_2$ with Different Particle Sizes as Attractive Positive Electrode Materials for Lithium-Ion Batteries: Insights into Their Structure. *J. Phys. Chem. C* **2012**, *116*, 13497–13506. https://doi.org/10.1021/jp301879x.
25. Jarvis, K.A.; Deng, Z.; Allard, L.F.; Manthiram, A.; Ferreira, P.J. Atomic Structure of a Lithium-Rich Layered Oxide Material for Lithium-Ion Batteries: Evidence of a Solid Solution. *Chem. Mater.* **2011**, *23*, 3614–3621. https://doi.org/10.1021/cm200831c.
26. Ates, M.N.; Mukerjee, S.; Abraham, K.M. A High Rate Li-Rich Layered MNC Cathode Material for Lithium-Ion Batteries. *RSC Adv.* **2015**, *5*, 27375–27386. https://doi.org/10.1039/c4ra17235c.
27. Boulineau, A.; Croguennec, L.; Delmas, C.; Weill, F. Structure of Li_2MnO_3 with Different Degrees of Defects. *Solid State Ion.* **2010**, *180*, 1652–1659. https://doi.org/10.1016/j.ssi.2009.10.020.
28. Lei, C.H.; Bareño, J.; Wen, J.G.; Petrov, I.; Kang, S.H.; Abraham, D.P. Local Structure and Composition Studies of $Li_{1.2}Ni_{0.2}Mn_{0.6}O_2$ by Analytical Electron Microscopy. *J. Power Sources* **2008**, *178*, 422–433. https://doi.org/10.1016/j.jpowsour.2007.11.077.

29. Tuccillo, M.; Costantini, A.; Celeste, A.; García, A.B.M.; Pavone, M.; Paolone, A.; Palumbo, O.; Brutti, S. NAi/Li Antisite Defects in the $Li_{1.2}Ni_{0.2}Mn_{0.6}O_2$ Li-Rich Layered Oxide: A DFT Study. *Crystals* **2022**, *12*, 723. https://doi.org/10.3390/cryst12050723.
30. Tang, Z.; Wang, S.; Liao, J.; Wang, S.; He, X.; Pan, B.; He, H.; Chen, C. Facilitating Lithium-Ion Diffusion in Layered Cathode Materials by Introducing Li^+/Ni^{2+} Antisite Defects for High-Rate Li-Ion Batteries. *Research* **2019**, *2019*, 2198906. https://doi.org/10.34133/2019/2198906.
31. Serrano-Sevillano, J.; Reynaud, M.; Saracibar, A.; Altantzis, T.; Bals, S.; van Tendeloo, G.; Casas-Cabanas, M. Enhanced Electrochemical Performance of Li-Rich Cathode Materials through Microstructural Control. *Phys. Chem. Chem. Phys.* **2018**, *20*, 23112–23122. https://doi.org/10.1039/c8cp04181d.
32. Matsunaga, T.; Komatsu, H.; Shimoda, K.; Minato, T.; Yonemura, M.; Kamiyama, T.; Kobayashi, S.; Kato, T.; Hirayama, T.; Ikuhara, Y.; et al. Dependence of Structural Defects in Li_2MnO_3 on Synthesis Temperature. *Chem. Mater.* **2016**, *28*, 4143–4150. https://doi.org/10.1021/acs.chemmater.5b05041.
33. Ma, D.; Li, Y.; Zhang, P.; Cooper, A.J.; Abdelkader, A.M.; Ren, X.; Deng, L. Mesoporous $Li_{1.2}Mn_{0.54}Ni_{0.13}Co_{0.13}O_2$ Nanotubes for High-Performance Cathodes in Li-Ion Batteries. *J. Power Sources* **2016**, *311*, 35–41. https://doi.org/10.1016/j.jpowsour.2016.01.031.
34. Buchholz, D.; Li, J.; Passerini, S.; Aquilanti, G.; Wang, D.; Giorgetti, M. X-Ray Absorption Spectroscopy Investigation of Lithium-Rich, Cobalt-Poor Layered-Oxide Cathode Material with High Capacity. *ChemElectroChem* **2015**, *2*, 85–97. https://doi.org/10.1002/celc.201402324.
35. Lu, Z.; Dahn, J.R. Understanding the Anomalous Capacity of $Li/Li[Ni_xLi_{(1/3-2x/3)}Mn_{(2/3-x/3)}]O_2$ Cells Using In Situ X-Ray Diffraction and Electrochemical Studies. *J. Electrochem. Soc.* **2002**, *149*, A815. https://doi.org/10.1149/1.1480014.
36. Zhao, S.; Yan, K.; Zhang, J.; Sun, B.; Wang, G. Reaction Mechanisms of Layered Lithium-Rich Cathode Materials for High-Energy Lithium-Ion Batteries. *Angew. Chem.—Int. Ed.* **2021**, *60*, 2208–2220.
37. Strehle, B.; Kleiner, K.; Jung, R.; Chesneau, F.; Mendez, M.; Gasteiger, H.A.; Piana, M. The Role of Oxygen Release from Li- and Mn-Rich Layered Oxides during the First Cycles Investigated by On-Line Electrochemical Mass Spectrometry. *J. Electrochem. Soc.* **2017**, *164*, A400–A406. https://doi.org/10.1149/2.1001702jes.
38. Armstrong, A.R.; Holzapfel, M.; Nová, P.; Johnson, C.S.; Kang, S.-H.; Thackeray, M.M.; Bruce, P.G. Demonstrating Oxygen Loss and Associated Structural Reorganization in the Lithium Battery Cathode $Li[Ni_{0.2}Li_{0.2}Mn_{0.6}]O_2$. *J. Am. Chem. Soc.* **2006**, *128*, 8694–8698. https://doi.org/10.1021/ja062027.
39. Sathiya, M.; Rousse, G.; Ramesha, K.; Laisa, C.P.; Vezin, H.; Sougrati, M.T.; Doublet, M.L.; Foix, D.; Gonbeau, D.; Walker, W.; et al. Reversible Anionic Redox Chemistry in High-Capacity Layered-Oxide Electrodes. *Nat. Mater.* **2013**, *12*, 827–835. https://doi.org/10.1038/nmat3699.
40. Sathiya, M.; Ramesha, K.; Rousse, G.; Foix, D.; Gonbeau, D.; Prakash, A.S.; Doublet, M.L.; Hemalatha, K.; Tarascon, J.M. High Performance $Li_2Ru_{1-y}Mn_yO_3$ ($0.2 \le y \le 0.8$) Cathode Materials for Rechargeable Lithium-Ion Batteries: Their Understanding. *Chem. Mater.* **2013**, *25*, 1121–1131. https://doi.org/10.1021/cm400193m.
41. Li, X.; Qiao, Y.; Guo, S.; Xu, Z.; Zhu, H.; Zhang, X.; Yuan, Y.; He, P.; Ishida, M.; Zhou, H. Direct Visualization of the Reversible O^{2-}/O^- Redox Process in Li-Rich Cathode Materials. *Adv. Mater.* **2018**, *30*, 1705197. https://doi.org/10.1002/adma.201705197.
42. Chen, H.; Islam, M.S. Lithium Extraction Mechanism in Li-Rich Li_2MnO_3 Involving Oxygen Hole Formation and Dimerization. *Chem. Mater.* **2016**, *28*, 6656–6663. https://doi.org/10.1021/acs.chemmater.6b02870.
43. Luo, K.; Roberts, M.R.; Guerrini, N.; Tapia-Ruiz, N.; Hao, R.; Massel, F.; Pickup, D.M.; Ramos, S.; Liu, Y.S.; Guo, J.; et al. Anion Redox Chemistry in the Cobalt Free 3d Transition Metal Oxide Intercalation Electrode $Li[Li_{0.2}Ni_{0.2}Mn_{0.6}]O_2$. *J. Am. Chem. Soc.* **2016**, *138*, 11211–11218. https://doi.org/10.1021/jacs.6b05111.
44. Luo, K.; Roberts, M.R.; Hao, R.; Guerrini, N.; Pickup, D.M.; Liu, Y.S.; Edström, K.; Guo, J.; Chadwick, A. v.; Duda, L.C.; et al. Charge-Compensation in 3d-Transition-Metal-Oxide Intercalation Cathodes through the Generation of Localized Electron Holes on Oxygen. *Nat. Chem.* **2016**, *8*, 684–691. https://doi.org/10.1038/nchem.2471.
45. Gent, W.E.; Lim, K.; Liang, Y.; Li, Q.; Barnes, T.; Ahn, S.J.; Stone, K.H.; McIntire, M.; Hong, J.; Song, J.H.; et al. Coupling between Oxygen Redox and Cation Migration Explains Unusual Electrochemistry in Lithium-Rich Layered Oxides. *Nat. Commun.* **2017**, *8*, 2091. https://doi.org/10.1038/s41467-017-02041-x.
46. Fell, C.R.; Qian, D.; Carroll, K.J.; Chi, M.; Jones, J.L.; Meng, Y.S. Correlation between Oxygen Vacancy, Microstrain, and Cation Distribution in Lithium-Excess Layered Oxides during the First Electrochemical Cycle. *Chem. Mater.* **2013**, *25*, 1621–1629. https://doi.org/10.1021/cm4000119.
47. Zuo, W.; Luo, M.; Liu, X.; Wu, J.; Liu, H.; Li, J.; Winter, M.; Fu, R.; Yang, W.; Yang, Y. Li-Rich Cathodes for Rechargeable Li-Based Batteries: Reaction Mechanisms and Advanced Characterization Techniques. *Energy Environ. Sci* **2020**, *13*, 4450–4497.
48. Assat, G.; Foix, D.; Delacourt, C.; Iadecola, A.; Dedryvère, R.; Tarascon, J.M. Fundamental Interplay between Anionic/Cationic Redox Governing the Kinetics and Thermodynamics of Lithium-Rich Cathodes. *Nat. Commun.* **2017**, *8*, 2219. https://doi.org/10.1038/s41467-017-02291-9.
49. Tao, S.; Huang, W.; Chu, S.; Qian, B.; Liu, L.; Xu, W. Dynamic Structural Evolution of Oxygen Vacancies in Lithium Rich Layered Composites Cathodes for Li-Ion Batteries. *Mater. Today Phys.* **2021**, *18*, 100403. https://doi.org/10.1016/j.mtphys.2021.100403.
50. Cui, S.L.; Wang, Y.Y.; Liu, S.; Li, G.R.; Gao, X.P. Evolution Mechanism of Phase Transformation of Li-Rich Cathode Materials in Cycling. *Electrochim Acta* **2019**, *328*, 135109. https://doi.org/10.1016/j.electacta.2019.135109.
51. Xu, B.; Fell, C.R.; Chi, M.; Meng, Y.S. Identifying Surface Structural Changes in Layered Li-Excess Nickel Manganese Oxides in High Voltage Lithium Ion Batteries: A Joint Experimental and Theoretical Study. *Energy Environ. Sci.* **2011**, *4*, 2223. https://doi.org/10.1039/c1ee01131f.

52. Boulineau, A.; Simonin, L.; Colin, J.F.; Bourbon, C.; Patoux, S. First Evidence of Manganese-Nickel Segregation and Densification upon Cycling in Li-Rich Layered Oxides for Lithium Batteries. *Nano Lett.* **2013**, *13*, 3857–3863. https://doi.org/10.1021/nl4019275.
53. Koga, H.; Croguennec, L.; Ménétrier, M.; Douhil, K.; Belin, S.; Bourgeois, L.; Suard, E.; Weill, F.; Delmas, C. Reversible Oxygen Participation to the Redox Processes Revealed for $Li_{1.20}Mn_{0.54}Co_{0.13}Ni_{0.13}O_2$. *J. Electrochem. Soc.* **2013**, *160*, A786–A792. https://doi.org/10.1149/2.038306jes.
54. Koga, H.; Croguennec, L.; Ménétrier, M.; Mannessiez, P.; Weill, F.; Delmas, C. Different Oxygen Redox Participation for Bulk and Surface: A Possible Global Explanation for the Cycling Mechanism of $Li_{1.20}Mn_{0.54}Co_{0.13}Ni_{0.13}O_2$. *J. Power Sources* **2013**, *236*, 250–258. https://doi.org/10.1016/j.jpowsour.2013.02.075.
55. Celeste, A.; Girardi, F.; Gigli, L.; Pellegrini, V.; Silvestri, L.; Brutti, S. Impact of Overlithiation and Al Doping on the Battery Performance of Li-Rich Layered Oxide Materials. *Electrochim Acta* **2022**, *428*, 140737. https://doi.org/10.1016/j.electacta.2022.140737.
56. Celeste, A.; Brescia, R.; Gigli, L.; Plaisier, J.; Pellegrini, V.; Silvestri, L.; Brutti, S. Unravelling Structural Changes of the $Li_{1.2}Mn_{0.54}Ni_{0.13}Co_{0.13}O_2$ Lattice upon Cycling in Lithium Cell. *Mater. Today Sustain.* **2022**, *21*, 100277. https://doi.org/10.1016/j.mtsust.2022.100277.
57. Armstrong, A.R.; Robertson, A.D.; Bruce, P.G. Overcharging Manganese Oxides: Extracting Lithium beyond Mn^{4+}. *J. Power Sources* **2005**, *146*, 275–280.
58. Gao, Y.; Wang, X.; Ma, J.; Wang, Z.; Chen, L. Selecting Substituent Elements for Li-Rich Mn-Based Cathode Materials by Density Functional Theory (DFT) Calculations. *Chem. Mater.* **2015**, *27*, 3456–3461. https://doi.org/10.1021/acs.chemmater.5b00875.
59. Hu, E.; Yu, X.; Lin, R.; Bi, X.; Lu, J.; Bak, S.; Nam, K.W.; Xin, H.L.; Jaye, C.; Fischer, D.A.; et al. Evolution of Redox Couples in Li- and Mn-Rich Cathode Materials and Mitigation of Voltage Fade by Reducing Oxygen Release. *Nat. Energy* **2018**, *3*, 690–698. https://doi.org/10.1038/s41560-018-0207-z.
60. Gu, M.; Belharouak, I.; Zheng, J.; Wu, H.; Xiao, J.; Genc, A.; Amine, K.; Thevuthasan, S.; Baer, D.R.; Zhang, J.G.; et al. Formation of the Spinel Phase in the Layered Composite Cathode Used in Li-Ion Batteries. *ACS Nano* **2013**, *7*, 760–767. https://doi.org/10.1021/nn305065u.
61. Hong, J.; Seo, D.H.; Kim, S.W.; Gwon, H.; Oh, S.T.; Kang, K. Structural Evolution of Layered $Li_{1.2}Ni_{0.2}Mn_{0.6}O_2$ upon Electrochemical Cycling in a Li Rechargeable Battery. *J. Mater. Chem.* **2010**, *20*, 10179–10186. https://doi.org/10.1039/c0jm01971b.
62. Yin, W.; Grimaud, A.; Rousse, G.; Abakumov, A.M.; Senyshyn, A.; Zhang, L.; Trabesinger, S.; Iadecola, A.; Foix, D.; Giaume, D.; et al. Structural Evolution at the Oxidative and Reductive Limits in the First Electrochemical Cycle of $Li_{1.2}Ni_{0.13}Mn_{0.54}Co_{0.13}O_2$. *Nat. Commun.* **2020**, *11*, 1252. https://doi.org/10.1038/s41467-020-14927-4.
63. Robertson, A.D.; Bruce, P.G. Overcapacity of $Li[Ni_xLi_{1/3-2x/3}Mn_{2/3-x/3}]O_2$ Electrodes. *Electrochem. Solid-State Lett.* **2004**, *7*, A294–A298. https://doi.org/10.1149/1.1783114.
64. Committee of the Regions and the European Investment Bank on the Implementation of the Strategic Action Plan on Batteries: Building a Strategic Battery Value Chain in Europe, https://eur-lex.europa.eu/legal-content/EN/TXT/HTML/?uri=CELEX:52019DC0176&rid=4, 09/04/2019.
65. GROW—Internal Market, D.D. *245 Final COMMISSION STAFF WORKING DOCUMENT Report on Raw Materials for Battery Applications*, https://www.europarl.europa.eu/doceo/document/A-9-2022-0031_EN.html, 17/05/2018.
66. Kugel', K.I.; Khomskii, D.I., The Jahn-Teller effect and magnetism: transition metal compounds, Sov. Phys. Usp. 25(4), April 1982, https://doi.org/10.1070/PU1982v025n04ABEH004537.
67. Tuccillo, M.; Mei, L.; Palumbo, O.; Muñoz-García, A.B.; Pavone, M.; Paolone, A.; Brutti, S. Replacement of Cobalt in Lithium-Rich Layered Oxides by n-Doping: A Dft Study. *Appl. Sci.* **2021**, *11*, 10545. https://doi.org/10.3390/app112210545.
68. Kou, J.; Chen, L.; Su, Y.; Bao, L.; Wang, J.; Li, N.; Li, W.; Wang, M.; Chen, S.; Wu, F. Role of Cobalt Content in Improving the Low-Temperature Performance of Layered Lithium-Rich Cathode Materials for Lithium-Ion Batteries. *ACS Appl. Mater. Interfaces* **2015**, *7*, 17910–17918. https://doi.org/10.1021/acsami.5b04514.
69. Ramesha, R.N.; Bosubabu, D.; Karthick Babu, M.G.; Ramesha, K. Tuning of Ni, Mn, and Co (NMC) Content in $0.4(LiNi_xMn_yCo_zO_2)\cdot 0.4(Li_2MnO_3)$ toward Stable High-Capacity Lithium-Rich Cathode Materials. *ACS Appl. Energy Mater.* **2020**, *3*, 10872–10881. https://doi.org/10.1021/acsaem.0c01897.
70. Redel, K.; Kulka, A.; Plewa, A.; Molenda, J. High-Performance Li-Rich Layered Transition Metal Oxide Cathode Materials for Li-Ion Batteries. *J. Electrochem. Soc.* **2019**, *166*, A5333–A5342. https://doi.org/10.1149/2.0511903jes.
71. Hamad, K.I.; Xing, Y. Effect of Cobalt and Nickel Contents on the Performance of Lithium Rich Materials Synthesized in Glycerol Solvent. *J. Electrochem. Soc.* **2018**, *165*, A2470–A2475. https://doi.org/10.1149/2.0311811jes.
72. Bao, L.; Yang, Z.; Chen, L.; Su, Y.; Lu, Y.; Li, W.; Yuan, F.; Dong, J.; Fang, Y.; Ji, Z.; et al. The Effects of Trace Yb Doping on the Electrochemical Performance of Li-Rich Layered Oxides. *ChemSusChem* **2019**, *12*, 2294–2301. https://doi.org/10.1002/cssc.201900226.
73. Kou, Y.; Han, E.; Zhu, L.Z.; Liu, L.; Zhang, Z. The Effect of Ti Doping on Electrochemical Properties of $Li_{1.167}Ni_{0.4}Mn_{0.383}Co_{0.05}O_2$ for Lithium-Ion Batteries. *Solid State Ion.* **2016**, *296*, 154–157. https://doi.org/10.1016/j.ssi.2016.09.020.
74. Guo, H.; Xia, Y.; Zhao, H.; Yin, C.; Jia, K.; Zhao, F.; Liu, Z. Stabilization Effects of Al Doping for Enhanced Cycling Performances of Li-Rich Layered Oxides. *Ceram. Int.* **2017**, *43*, 13845–13852. https://doi.org/10.1016/j.ceramint.2017.07.107.
75. Tang, T.; Zhang, H.L. Synthesis and Electrochemical Performance of Lithium-Rich Cathode Material $Li[Li_{0.2}Ni_{0.15}Mn_{0.55}Co_{0.1-x}Al_x]O_2$. *Electrochim. Acta* **2016**, *191*, 263–269. https://doi.org/10.1016/j.electacta.2016.01.066.

76. Dong, S.; Zhou, Y.; Hai, C.; Zeng, J.; Sun, Y.; Shen, Y.; Li, X.; Ren, X.; Sun, C.; Zhang, G.; et al. Understanding Electrochemical Performance Improvement with Nb Doping in Lithium-Rich Manganese-Based Cathode Materials. *J. Power Sources* **2020**, *462*, 228185. https://doi.org/10.1016/j.jpowsour.2020.228185.
77. Liu, X.; Yu, B.; Wang, M.; Jin, Y.; Fu, Z.; Chen, J.; Ma, Z.; Guo, B.; Huang, Y.; Li, X. Electrochemical Performances of Niobium-Doped New Spherical Low-Cobalt Li-Rich Mn-Based $Li_{1.14}Mn_{0.476}Ni_{0.254}Co_{0.048}Al_{0.016}O_2$ Cathode. *Mater. Today Commun.* **2022**, *32*, 104170. https://doi.org/10.1016/j.mtcomm.2022.104170.
78. Nayak, P.K.; Grinblat, J.; Levi, M.; Haik, O.; Levi, E.; Aurbach, D. Effect of Fe in Suppressing the Discharge Voltage Decay of High Capacity Li-Rich Cathodes for Li-Ion Batteries. *J. Solid State Electrochem.* **2015**, *19*, 2781–2792. https://doi.org/10.1007/s10008-015-2790-2.
79. Yi, T.F.; Li, Y.M.; Cai, X.D.; Yang, S.Y.; Zhu, Y.R. Fe-Stabilized Li-Rich Layered $Li_{1.2}Mn_{0.56}Ni_{0.16}Co_{0.08}O_2$ Oxide as a High Performance Cathode for Advanced Lithium-Ion Batteries. *Mater. Today Energy* **2017**, *4*, 25–33. https://doi.org/10.1016/j.mtener.2017.03.005.
80. Medvedeva, A.; Makhonina, E.; Pechen, L.; Politov, Y.; Rumyantsev, A.; Koshtyal, Y.; Goloveshkin, A.; Maslakov, K.; Eremenko, I. Effect of Al and Fe Doping on the Electrochemical Behavior of $Li_{1.2}Ni_{0.133}Mn_{0.534}Co_{0.133}O_2$ Li-Rich Cathode Material. *Materials* **2022**, *15*, 8225. https://doi.org/10.3390/ma15228225.
81. Nisar, U.; Amin, R.; Shakoor, A.; Essehli, R.; Al-Qaradawi, S.; Kahraman, R.; Belharouak, I. Synthesis and Electrochemical Characterization of Cr-Doped Lithium-Rich $Li_{1.2}Ni_{0.16}Mn_{0.56}Co_{0.08-x}Cr_xO_2$ Cathodes. *Emergent Mater.* **2018**, *1*, 155–164. https://doi.org/10.1007/s42247-018-0014-0.
82. Ghorbanzadeh, M.; Allahyari, E.; Riahifar, R.; Hadavi, S.M.M. Effect of Al and Zr Co-Doping on Electrochemical Performance of Cathode $Li[Li_{0.2}Ni_{0.13}Co_{0.13}Mn_{0.54}]O_2$ for Li-Ion Battery. *J. Solid State Electrochem.* **2018**, *22*, 1155–1163. https://doi.org/10.1007/s10008-017-3824-8.
83. Celeste, A.; Brescia, R.; Greco, G.; Torelli, P.; Mauri, S.; Silvestri, L.; Pellegrini, V.; Brutti, S. Pushing Stoichiometries of Lithium-Rich Layered Oxides Beyond Their Limits. *ACS Appl. Energy Mater.* **2022**, *5*, acsaem.1c03396. https://doi.org/10.1021/acsaem.1c03396.
84. Feng, Z.; Song, H.; Li, Y.; Lyu, Y.; Xiao, D.; Guo, B. Adjusting Oxygen Redox Reaction and Structural Stability of Li- and Mn-Rich Cathodes by Zr-Ti Dual-Doping. *ACS Appl. Mater. Interfaces* **2022**, *14*, 5308–5317. https://doi.org/10.1021/acsami.1c20880.
85. Zhang, H.Z.; Qiao, Q.Q.; Li, G.R.; Gao, X.P. PO_4^{3-} Polyanion-Doping for Stabilizing Li-Rich Layered Oxides as Cathode Materials for Advanced Lithium-Ion Batteries. *J. Mater. Chem. A Mater.* **2014**, *2*, 7454–7460. https://doi.org/10.1039/c4ta00699b.
86. Zhang, H.-Z.; Li, F.; Pan, G.-L.; Li, G.-R.; Gao, X.-P. The Effect of Polyanion-Doping on the Structure and Electrochemical Performance of Li-Rich Layered Oxides as Cathode for Lithium-Ion Batteries. *J. Electrochem. Soc.* **2015**, *162*, A1899–A1904. https://doi.org/10.1149/2.1031509jes.
87. Kang, S.H.; Sun, Y.K.; Amine, K. Electrochemical and Ex Situ X-ray Study of $Li(Li_{0.2}Ni_{0.2}Mn_{0.6})O_2$ Cathode Material for Li Secondary Batteries. *Electrochem. Solid-State Lett.* **2003**, *6*, A183–A186. https://doi.org/10.1149/1.1594411.
88. Rajappa Prakasha, K.; Grins, J.; Jaworski, A.; Thersleff, T.; Svensson, G.; Jøsang, L.O.; Dyrli, A.D.; Paulus, A.; de Sloovere, D.; D'Haen, J.; et al. Temperature-Driven Chemical Segregation in Co-Free Li-Rich-Layered Oxides and Its Influence on Electrochemical Performance. *Chem. Mater.* **2022**, *34*, 3637–3647. https://doi.org/10.1021/acs.chemmater.1c04150.
89. Laisa, C.P.; Nanda Kumar, A.K.; Selva Chandrasekaran, S.; Murugan, P.; Lakshminarasimhan, N.; Govindaraj, R.; Ramesha, K. A Comparative Study on Electrochemical Cycling Stability of Lithium Rich Layered Cathode Materials $Li_{1.2}Ni_{0.13}M_{0.13}Mn_{0.54}O_2$ Where M = Fe or Co. *J. Power Sources* **2016**, *324*, 462–474. https://doi.org/10.1016/J.JPOWSOUR.2016.05.107.
90. Wu, F.; Kim, G.T.; Kuenzel, M.; Zhang, H.; Asenbauer, J.; Geiger, D.; Kaiser, U.; Passerini, S. Elucidating the Effect of Iron Doping on the Electrochemical Performance of Cobalt-Free Lithium-Rich Layered Cathode Materials. *Adv. Energy Mater.* **2019**, *9*, 1902445. https://doi.org/10.1002/aenm.201902445.
91. Wei, H.; Cheng, X.; Fan, H.; Shan, Q.; An, S.; Qiu, X.; Jia, G. A Cobalt-Free $Li(Li_{0.17}Ni_{0.17}Fe_{0.17}Mn_{0.49})O_2$ Cathode with More Oxygen-Involving Charge Compensation for Lithium-Ion Batteries. *ChemSusChem* **2019**, *12*, 2471–2479. https://doi.org/10.1002/cssc.201900241.
92. Pham, H.Q.; Kondracki, Ł.; Tarik, M.; Trabesinger, S. Correlating the Initial Gas Evolution and Structural Changes to Cycling Performance of Co-Free Li-Rich Layered Oxide Cathode. *J. Power Sources* **2022**, *527*, 231181. https://doi.org/10.1016/j.jpowsour.2022.231181.
93. Lu, Z.; Dahn, J.R. Structure and Electrochemistry of Layered $Li[Cr_{(1/3-x/3)}Mn_{(2/3-2x/3)}]O_2$. *J. Electrochem. Soc.* **2002**, *149*, A1454. https://doi.org/10.1149/1.1513557.
94. Sun, Y.K.; Kim, M.G.; Kang, S.H.; Amine, K. Electrochemical Performance of Layered $Li[Li_{0.15}Ni_{0.275-x}Mg_xMn_{0.575}]O_2$ Cathode Materials for Lithium Secondary Batteries. *J. Mater. Chem.* **2003**, *13*, 319–322. https://doi.org/10.1039/B209379K.
95. Wang, D.; Huang, Y.; Huo, Z.; Chen, L. Synthesize and Electrochemical Characterization of Mg-Doped Li-Rich Layered $Li[Li_{0.2}Ni_{0.2}Mn_{0.6}]O_2$ Cathode Material. *Electrochim. Acta* **2013**, *107*, 461–466. https://doi.org/10.1016/J.ELECTACTA.2013.05.145.
96. Celeste, A.; Tuccillo, M.; Santoni, A.; Reale, P.; Brutti, S.; Silvestri, L. Exploring a Co-Free, Li-Rich Layered Oxide with Low Content of Nickel as a Positive Electrode for Li-Ion Battery. *ACS Appl. Energy Mater.* **2021**, *4*, 11290–11297. https://doi.org/10.1021/acsaem.1c02133.
97. Vanaphuti, P.; Bong, S.; Ma, L.; Ehrlich, S.; Wang, Y. Systematic Study of Different Anion Doping on the Electrochemical Performance of Cobalt-Free Lithium-Manganese-Rich Layered Cathode. *ACS Appl. Energy Mater.* **2020**, *3*, 4852–4859. https://doi.org/10.1021/acsaem.0c00439.

98. Liu, H.; He, B.; Xiang, W.; Li, Y.C.; Bai, C.; Liu, Y.P.; Zhou, W.; Chen, X.; Liu, Y.; Gao, S.; et al. Synergistic Effect of Uniform Lattice Cation/Anion Doping to Improve Structural and Electrochemical Performance Stability for Li-Rich Cathode Materials. *Nanotechnology* **2020**, *31*, 455704. https://doi.org/10.1088/1361-6528/ab9579.
99. Nie, L.; Wang, Z.; Zhao, X.; Chen, S.; He, Y.; Zhao, H.; Gao, T.; Zhang, Y.; Dong, L.; Kim, F.; et al. Cation/Anion Codoped and Cobalt-Free Li-Rich Layered Cathode for High-Performance Li-Ion Batteries. *Nano Lett.* **2021**, *21*, 8370–8377. https://doi.org/10.1021/ACS.NANOLETT.1C02923/ASSET/IMAGES/LARGE/NL1C02923_0005.JPEG.
100. Thackeray, M.M.; Kang, S.H.; Johnson, C.S.; Vaughey, J.T.; Hackney, S.A. Comments on the Structural Complexity of Lithium-Rich $Li_{1+x}M_{1-x}O_2$ Electrodes (M = Mn, Ni, Co) for Lithium Batteries. *Electrochem. Commun.* **2006**, *8*, 1531–1538. https://doi.org/10.1016/j.elecom.2006.06.030.
101. Wang, C.C.; Jarvis, K.A.; Ferreira, P.J.; Manthiram, A. Effect of Synthesis Conditions on the First Charge and Reversible Capacities of Lithium-Rich Layered Oxide Cathodes. *Chem. Mater.* **2013**, *25*, 3267–3275. https://doi.org/10.1021/cm402181f.
102. Deng, Z.Q.; Manthiram, A. Influence of Cationic Substitutions on the Oxygen Loss and Reversible Capacity of Lithium-Rich Layered Oxide Cathodes. *J. Phys. Chem. C* **2011**, *115*, 7097–7103. https://doi.org/10.1021/JP200375D/ASSET/IMAGES/LARGE/JP-2011-00375D_0015.JPEG.
103. Wang, C.C.; Manthiram, A. Influence of Cationic Substitutions on the First Charge and Reversible Capacities of Lithium-Rich Layered Oxide Cathodes. *J. Mater. Chem. A Mater.* **2013**, *1*, 10209–10217. https://doi.org/10.1039/C3TA11703K.
104. Lee, E.; Park, J.S.; Wu, T.; Sun, C.J.; Kim, H.; Stair, P.C.; Lu, J.; Zhou, D.; Johnson, C.S. Role of Cr^{3+}/Cr^{6+} Redox in Chromium-Substituted $Li_2MnO_3{\cdot}LiNi_{1/2}Mn_{1/2}O_2$ Layered Composite Cathodes: Electrochemistry and Voltage Fade. *J. Mater. Chem. A Mater.* **2015**, *3*, 9915–9924. https://doi.org/10.1039/C5TA01214G.